Visible-light photoconductivity of Zn_{1-x}Co_{x}O and its dependence on Co^{2+} concentration

Claire A. Johnson, Alicia Cohn, Tiffany Kaspar, Scott A. Chambers, G. Mackay Salley, and Daniel R. Gamelin

Phys. Rev. B **84**, 125203 — Published 6 September 2011

DOI: 10.1103/PhysRevB.84.125203

June 16, 2011

Visible-Light Photoconductivity of $Zn_{1-x}Co_xO$ and its Dependence on Co^{2+} Concentration

Claire A. Johnson,[1] Alicia Cohn,[1] Tiffany Kaspar,[2] Scott A. Chambers,[2] G. Mackay Salley,[1,3] and Daniel R. Gamelin[1,*]

[1]*Department of Chemistry, University of Washington, Seattle, WA 98195-1700*

[2]*Pacific Northwest National Laboratory, Richland, WA 99352*

[3]*Department of Physics, Wofford College, Spartanburg, SC 29303*

E-mail: Gamelin@chem.washington.edu

Abstract. Many metal oxides investigated for solar photocatalysis or photoelectrochemistry have band gaps that are too wide to absorb a sufficient portion of the solar spectrum. Doping with impurity ions has been extensively explored as a strategy to sensitize such oxides to visible light, but the electronic structures of the resulting materials are frequently complex and poorly understood. Here, we report a detailed photoconductivity investigation of the wide-gap II-VI semiconductor ZnO doped with Co^{2+} ($Zn_{1-x}Co_xO$), which responds to visible light in photoelectrochemical and photoconductivity experiments and thus represents a well-defined model system for understanding dopant-sensitized oxides. Variable-temperature scanning photoconductivity measurements have been performed on $Zn_{1-x}Co_xO$ epitaxial films to examine the relationship between dopant concentration (x) and visible-light photoconductivity, with particular focus on mid-gap intra-d-shell (*d*-*d*) photoactivity. Excitation into the intense $^4T_1(P)$ *d*-*d* band at ~2.0 eV (620 nm) leads to $Co^{2+/3+}$ ionization with a quantum efficiency that increases with decreasing cobalt concentration and increasing sample temperature. Both spontaneous and thermally assisted ionization from the Co^{2+} *d*-*d* excited state are found to become less effective as x is increased, attributed to an increasing conduction-band-edge potential. These trends counter the increasing light absorption with increasing x, explaining the experimental maximum in external photon-to-current conversion efficiencies at values well below the solid solubility of Co^{2+} in ZnO.

Introduction

Doping wide-gap oxide semiconductors (*e.g.*, TiO_2, ZnO, $InTaO_4$) with impurity ions (*e.g.*, N^{3-}, S^{2-}, Fe^{3+}, Cr^{3+}, Co^{2+}) frequently extends their photo-responses into the visible spectral range, and has been actively explored as a means of enabling such materials to become useful for conversion of solar energy into chemical or electrical potentials.[1-14] Mid-gap photoactivity is usually associated with donor- or acceptor-type photoionization (or charge-transfer) transitions

of the added impurity ions. Such transitions can generate one band-like charge carrier (either a conduction-band electron or a valence-band hole) by formal charge transfer from or to the impurity. The real electronic structures of such solid solutions are complex, however, and generally, little is known about the ionization potentials of the impurities relative to the band-edge potentials of the host oxides, or about the impact of impurity incorporation on these band-edge potentials.

In some cases, mid-gap photoactivity is observed that appears to result from excitation of highly localized transitions, such as the intra-*d*-shell (*d-d*) transitions of transition-metal impurities. For example, photoelectrochemical water reduction and H_2 evolution has been reported from Co^{2+}-doped ZnO ($Zn_{1-x}Co_xO$) following excitation into the Co^{2+} *d-d* transition at ~2.0 eV,[10] deep within the ZnO energy gap (~3.4 eV). Similarly, excitation of Cr^{3+}-centered *d-d* transitions in Cr^{3+}/Sb^{5+}-codoped TiO_2 has been reported to induce O_2 evolution from aqueous silver nitrate solutions,[6] and doping $InTaO_4$ with Ni^{2+} reportedly yields a colored material that produces hydrogen from water when a Ni^{2+} *d-d* transition is irradiated with visible light.[3] Such *d-d* photoactivity is not well understood in these cases, and at first sight is incongruous with the small localization lengths of *d-d* excited states.

In this study, we use photoconductivity measurements to examine the microscopic origins of the *d-d* photoactivity of $Zn_{1-x}Co_xO$, which in many ways serves as a model doped oxide for understanding this class of materials as a whole. The unusual observation of mid-gap photoconductivity resulting from *d-d* excitation of $Zn_{1-x}Co_xO$ was first reported by Kanai in 1968,[15] and has been investigated many times subsequently.[10,11,16-23] This observation is unusual because photoconductivity selectively probes the excited states of a material that generate mobile charge carriers, *i.e.*, a photocurrent.[24,25] In semiconductors, these are generally band-to-band

transitions, but may also include mid-gap impurity photoionization transitions. *d-d* transitions are local by nature and cannot directly generate mobile charge carriers. For this reason, *d-d* transitions of transition-metal ions in semiconductors are adequately described by ligand-field theory, and hence are commonly denoted using the standard multi-electron term symbols for the appropriate cation site symmetry.[26,27]

After over 40 years of study, the *d-d* photoconductivity of $Zn_{1-x}Co_xO$ is still not fully understood. From the original observations, Kanai concluded that the Co^{2+} $^4T_1(P)$ excited state must be located "near or in the conduction band of ZnO".[15] In other words, *d-d* photoexcitation must be followed by electron transfer into the ZnO conduction band. Photoluminescence from this manifold of *d-d* states is sometimes observed, however, and this observation has been used to suggest that the *d-d* origin resides below the $Co^{2+/3+}$ ionization threshold in ZnO.[28] In some studies, photo-thermal ionization has been suggested,[18,19,22] and in others the $^4T_1(P)$ absorption band does *not* produce any photoconductivity signal,[23] as might have been expected for a localized *d-d* excitation. The precise locations of the Co^{2+} ionization thresholds relative to the ZnO band edges thus remain poorly defined, although these relationships are of central importance not just to photoconductivity but also to the magnetic properties of this same material.[29-33]

Theory has not resolved this aspect of the $Zn_{1-x}Co_xO$ electronic structure either. Consensus has not been reached on whether the empty t_2 orbitals of the $^4A_2$ ground state reside inside the conduction band,[31,33] are degenerate with the conduction-band edge,[32] or can reside below it when associated with an oxygen vacancy.[31]

Moreover, several groups have reported that the *d-d* photoresponse of $Zn_{1-x}Co_xO$ does not simply increase with increasing x, as the *d-d* absorbance does.[10-12,20,21] Instead, the photoresponse

of $Zn_{1-x}Co_xO$ is generally found to maximize at relatively small values of x (between 0.02 and 0.05), well below usual solid solubility limits for Co^{2+} in the wurtzite lattice structure (up to ~0.50[34]). This discrepancy has been explained in terms of increased electron scattering at large x coming either from impurity phase segregation[21] or from reduced crystallinity.[10] Complicating the interpretation of this observation is the fact that prior studies have focused on polycrystalline $Zn_{1-x}Co_xO$, and have been limited to room temperature.[10-12,15-17,20,21]

Here, we describe results from a systematic investigation into the role of Co^{2+} concentration on *d-d* photoresponse in $Zn_{1-x}Co_xO$. Variable-temperature scanning photoconductivity measurements have been performed on a series of high-structural-quality $Zn_{1-x}Co_xO$ epitaxial films. The use of these epitaxial films minimizes the roles of surfaces and grain boundaries, and hence allows reliable observation of the intrinsic electronic structure features of the $Zn_{1-x}Co_xO$. The data presented here demonstrate that the concentration dependence described above ultimately originates from a dependence of the conduction-band-edge potential on x that increases the $Co^{2+/3+}$ donor ionization energy relative to that of the $^4T_1(P)$ *d-d* excited state. In the limit of low Co^{2+} concentrations (x < ~0.01), ionization occurs at energies below the $^4A_2 \rightarrow {}^4T_1(P)$ origin, and *d-d* photoconductivity is readily observed. In the high-concentration limit (x > ~0.23), the $^4T_1(P)$ excited state resides well below the donor-type ionization threshold, and *d-d* photoconductivity is no longer observed. At intermediate values of x, spontaneous ionization following $^4T_1(P)$ excitation is hindered kinetically by the presence of an activation barrier to ionization, and thermally activated photoionization dominates. The *d-d* photoconductivity thus depends strongly on both temperature and Co^{2+} concentration in systematic ways. These results provide detailed insight into the visible-light sensitization of this

wide-gap semiconductor by Co^{2+} doping, and enrich our general understanding of impurity-doped semiconductors as a whole.

Methods

Epitaxial films of $Zn_{1-x}Co_xO$ were grown on *r*-Al_2O_3 and *c*-Al_2O_3 substrates by off-axis pulsed laser deposition (PLD) using polycrystalline $Zn_{1-x}Co_xO$ and ZnO targets as described previously.[35] Similar films prepared by this method have been characterized in detail elsewhere.[35-38] Briefly, epitaxial films of $Zn_{1-x}Co_xO$ were obtained from deposition onto both *c*-sapphire and *r*-sapphire. Atom-specific x-ray linear dichroism measurements on a set of films grown under identical conditions to those used here reveal that in excess of 95% of all cobalt dopants are at fully-coordinated zinc sites. Although grain boundaries are present due to lattice mismatch with the substrate, fewer than 5% of the cobalt dopants are located on internal surfaces associated with grain boundaries.[37,38] High-resolution X-ray diffraction (XRD) measurements exhibited narrow peak widths (0.057 – 0.139° θ), indicative of well-ordered crystallinity with little mosaic spread. X-ray absorption spectra confirm that Co^{2+} substitutes for Zn^{2+} in these films. High-resolution TEM images show sharp and abrupt *c*-$Zn_{1-x}Co_xO$/*c*-sapphire interfaces without misfit dislocations; the misfit strain is accommodated by grain boundaries between columns. For *a*-$Zn_{1-x}Co_xO$ on *r*-sapphire, the smaller lattice mismatch results in column-free growth with misfit dislocations at the ZnO/sapphire interfaces. No evidence has been found for any impurity phases within the detection limits of x-ray diffraction, x-ray absorption spectroscopy, and transmission electron microscopy. Energy-dispersive x-ray spectroscopy (EDX) did not detect cobalt segregation to the film surface or interface. Additional details are provided in refs. 35-38.

Photoconductivities of these epitaxial films were measured following methods detailed in Ref. 22. Briefly, indium-wrapped copper contacts were placed ~1 mm apart onto the surface of a film, voltage was applied (for all spectra shown, the applied voltages were 20 V), and the sample was excited from the front side with monochromatic light. A tungsten-halogen lamp dispersed through a 0.3 m monochromator equipped with a 600 gr/mm grating blazed at 500 nm was used as the excitation source. All data have been corrected for the lamp and monochromator output. Samples were excited using chopped (20 Hz) illumination, and photocurrents were detected using a Stanford Research SR830 lock-in amplifier. It was previously demonstrated that AC and DC photoconductivity measurements on such films yield very similar results.[22]

Variable-temperature photoconductivity measurements were performed using a Janis optical cryostat with the sample in flowing helium or nitrogen gas. Electronic absorption measurements were performed on a Cary 500 spectrophotometer (Varian). Interference fringes in electronic absorption spectra were corrected using the method of Ref. 39. The electronic absorption and photoconductivity data shown here are from measurements performed on the same films, except in the case of the $Zn_{0.96}Co_{0.04}O$ film, which was grown on a substrate polished only on one side. For this case, the absorption spectrum of another film with approximately the same *x* and film thickness is shown.

Results and Analysis

Figure 1a shows room-temperature electronic absorption spectra of epitaxial ZnO, $Zn_{0.98}Co_{0.02}O$, and $Zn_{0.9}Co_{0.11}O$ thin films. As detailed previously, three major features are observed in the energy window between ~1.5 and 4.0 eV: (*i*) the ZnO band-to-band absorption at ≥ ~3.22 eV, (*ii*) the $Co^{2+/+}$ acceptor-type photoionization (or valence-band-to-metal charge transfer (L_{VB}MCT)) transition between ~2.85 eV and ~3.22 eV,[11,30,40] and (*iii*) the structured $^4A_2 \rightarrow {}^4T_1(P)$ *d-d* band at ~2.0 eV (using term symbols of the parent tetrahedral point group).[41,42] Spin-orbit coupling splits this *d-d* band into four major components and also enables mixing of these components with the nearby doublet *d-d* states arising from the ^2G free-ion term, allowing the latter to gain electric dipole intensity in the electronic absorption experiment.[41,42] Because the electric dipole intensity of this band derives from its $^4A_2 \rightarrow {}^4T_1$ character, we refer to the entire absorption feature as the $^4T_1(P)$ band.

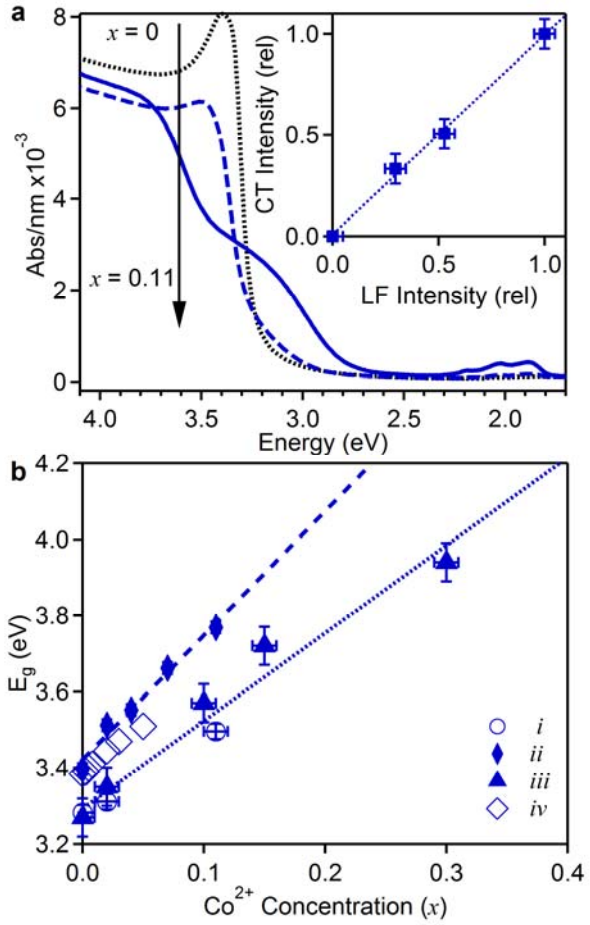

FIG. 1. (a) Room-temperature electronic absorption spectra of *c*-$Zn_{1-x}Co_xO$ thin films with $x = 0$, 0.02, and 0.11, normalized for film thickness. Inset: Integrated intensity of the L_{VB}MCT transition plotted *vs* the integrated $^4A_2(F) \rightarrow {}^4T_1(P)$ intensity for these three films and another having $x = 0.04$. **(b)** Energy of the first ZnO band-to-band transition (E_g) as a function of x. (*i*) this work, see text for analysis; (*ii*) this work, energy at the maximum of the exciton peak; (*iii*) Ivill *et al.*;[43] (*iv*) Xiao *et al.*[44] The dotted and dashed lines show linear best fits given by E_g (eV) = 3.29 + 2.305x (·····) and E_g (eV) = 3.41 + 3.56x (----).

A plot of the integrated L_{VB}MCT intensity versus the integrated $^4A_2 \rightarrow {}^4T_1(P)$ *d-d* intensity yields a linear relationship (Fig. 1a(inset)), as expected for two Co^{2+}-centered transitions. From these data, the oscillator strength of the L_{VB}MCT transition is roughly an order of magnitude greater than that of the *d-d* transition. With increasing x, the ZnO band-to-band absorption shifts to higher energy and decreases in intensity, while the L_{VB}MCT intensity

increases. The L_{VB}MCT transition of $Zn_{1-x}Co_xO$ at small x ultimately becomes the band-gap transition of the charge-transfer insulator *w*-CoO (*i.e.*, at $x = 1$).[45]

Figure 1b plots the dependence of the apparent energy gap on x for several $Zn_{1-x}Co_xO$ films from this work and from recent literature.[43,46] The specific energies shown here were determined either from the intersection of the excitonic and sub-bandgap absorption features in plots of $(\alpha h\nu)^2$ vs $h\nu$ (solid symbols) or from the maxima of the first band-to-band absorption feature (open symbols). In both methods, correction for the ~60 meV exciton binding energy is neglected. Both analyses show that the ZnO energy gap increases with increasing x, with $E_g \approx (3.4 + 3.0x)$ eV, in good agreement with most previous conclusions.[43,46-48] (In some instances a narrowing of the ZnO energy gap with x has been suggested,[49-52] but this suggestion arises from misinterpretation of the L_{VB}MCT intensity in samples that are too thick for observation of the band-to-band maximum.) Because the conduction band of ZnO is largely $Zn^{2+}(4s)$-based, removing Zn^{2+} and replacing it with Co^{2+} disproportionately impacts the conduction-band wavefunction.

Figure 2 compares room-temperature $Zn_{0.96}Co_{0.04}O$ electronic absorption and photoconductivity spectra in the *d-d* energy region. Both spectra are dominated by the prominent structured $^4A_2 \rightarrow {}^4T_1(P)$ band centered at ~2.0 eV. The weaker absorption feature at ~0.9 eV is the $^4A_2 \rightarrow {}^4T_1(F)$ band, also split by spin-orbit interactions.[41,42] The third spin-allowed *d-d* transition of Co^{2+}, $^4A_2 \rightarrow {}^4T_2(F)$, occurs at lower energy (~0.75 eV).[41,42] The photoconductivity measurements (Fig. 2b) show a clear response from excitation into the $^4T_1(P)$ band, but no photoconductivity is detected from excitation into the $^4T_1(F)$ or $^4T_2(F)$ bands. These data indicate that the $^4T_1(P)$ excited state is sufficiently energetic for Co^{2+} ionization to occur, but the lower *d-d* excited states are not. The contrast between the photoactivities of the $^4T_1(P)$ and $^4T_1(F)$ excited

states in Fig. 2 thus provides strong evidence that the *d-d* photoconductivity observed here actually involves sensitization of a nearby photoionization excited state. This situation has previously been interpreted as indicating that the $^4T_1(P)$ manifold overlaps the manifold of $Co^{2+/3+}$ donor-type photoionization states.[15,22] The latter has been observed in photocurrent measurements[11] but has a very low oscillator strength and hence is not readily distinguished from the baseline by electronic absorption spectroscopy. The remainder of this study will focus on understanding the photoconductivity observed with $^4T_1(P)$ excitation.

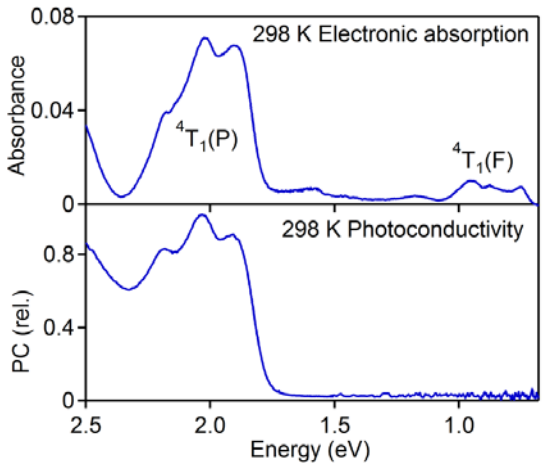

FIG. 2. Comparison of 298 K electronic absorption **(a)** and photoconductivity **(b)** spectra of an *a*-$Zn_{0.96}Co_{0.04}O$ thin film. Although the $^4T_1(P)$ *d-d* transition shows a photoconductivity response, the $^4T_2(F)$ *d-d* transition does not. Note that the absorption baseline is influenced by interference fringes and therefore does not appear flat between the two *d-d* bands.

Figure 3 compares the results of room-temperature visible-light photoconductivity and valence-band X-ray photoelectron spectroscopy (VB-XPS) measurements on $Zn_{1-x}Co_xO$ and ZnO epitaxial films. The VB-XPS spectra (Fig. 3a, adapted from Ref. [35]) have been aligned assuming that the Fermi energy is close to the CB in these *n*-type films, which puts the Zn^{2+} 3*d* peak at 10.04 eV.[35] Figure 3b shows an expanded view of the VB-XPS spectra near the onset of VB intensity. Addition of Co^{2+} leads to new XPS intensity inside the ZnO gap, suggesting the

presence of $Co^{2+/3+}$ donor levels above the valence band, as illustrated in Fig. 3c (left). Figure 3d shows room-temperature photoconductivity spectra of ZnO and $Zn_{1-x}Co_xO$ (x = 0.04) epitaxial films on the same energy scale as Fig. 3b. Photoconductivity measurements also show new intensity within the ZnO gap upon the introduction of Co^{2+}. The similarity between the photoconductivity and VB-XPS spectra provides strong evidence supporting association of this mid-gap photoconductivity with a $Co^{2+/3+}$ donor-type ionization transition,[11,22,30] as shown in Fig. 3c (right). As illustrated schematically in Fig. 3c, whereas VB-XPS probes the promotion of electrons from occupied orbitals to form high-energy continuum states, photoconductivity can probe excitation of the same electrons to the CB, and both experiments therefore yield complementary information about the relationship between VB and dopant ionization energies. Photoconductivity is additionally sensitive to acceptor-type ionization transitions, but these occur at higher energies (>~2.8 eV, see Fig. 1a) in $Zn_{1-x}Co_xO$[11,30,40] and are not the focus of the present study.

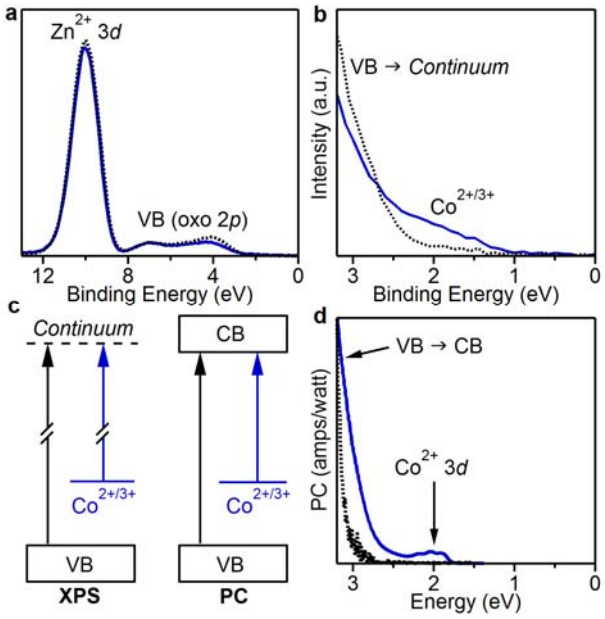

FIG. 3. (a) Room-temperature VB-XPS spectra of a-$Al_{0.01}Zn_{0.94}Co_{0.05}O$ (—) and a-$Al_{0.02}Zn_{0.98}O$ (···) films, adapted from Ref. [35]. **(b)** Data from (a) plotted on an expanded

scale. **(c)** Schematic summary of the VB-XPS and photoconductivity experiments. **(d)** Room-temperature photoconductivity spectra of *a*-ZnO (· · ·) and *a*-$Zn_{0.96}Co_{0.04}O$ (—) plotted on the same energy scale as (b).

Figure 4 compares the room-temperature electronic absorption and photoconductivity spectra of four different $Zn_{1-x}Co_xO$ films (x = 0.008, 0.04, 0.07, and 0.11) in the $^4T_1(P)$ energy region. Figure 4a shows the electronic absorption spectra of the four films, normalized for film thickness and corrected for interference fringes to the greatest extent possible. As expected, the $^4A_2 \rightarrow {}^4T_1(P)$ *d-d* absorption increases in proportion to x in these films (Fig. 4a,b), *i.e.*, films with greater x have a greater light harvesting efficiency (LHE) in the *d-d* spectral region.

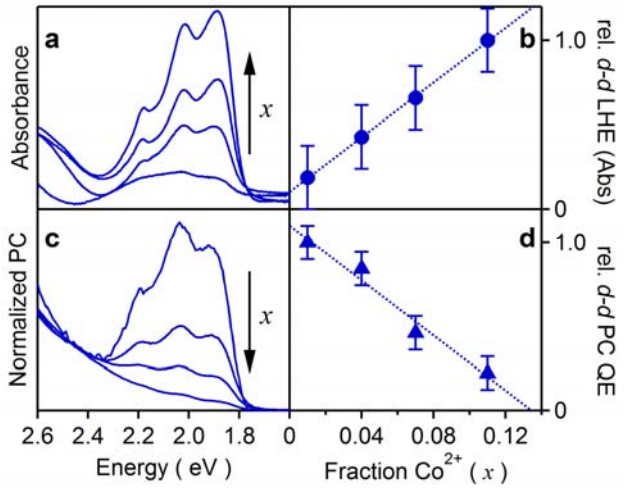

FIG. 4. (a) Room-temperature electronic absorption spectra of *a*-$Zn_{1-x}Co_xO$ films (x = 0.008, 0.04, 0.07, 0.11), normalized for film thickness (~500, ~300, ~400, and ~500 nm, respectively). The error bars reflect uncertainties due to interference fringes. **(b)** Integrated absorption in the *d-d* energy range (2.36 – 1.72 eV) of the spectra shown in (a), normalized to the largest value. **(c)** Room-temperature photoconductivity action spectra of *a*-$Zn_{1-x}Co_xO$ films (x = 0.008, 0.04, 0.07, 0.11), all normalized at 2.8 eV. **(d)** Integrated photoconductivity in the *d-d* energy range (2.36 – 1.72 eV) of the spectra shown in (c), normalized to the largest value.

Paradoxically, photoconductivity measurements show the opposite trend. Figure 4c plots room-temperature photoconductivity action spectra for this series of $Zn_{1-x}Co_xO$ films, normalized in the $Co^{2+/+}$ charge-transfer region (2.8 eV).[40] This normalization procedure facilitates

comparison of films with different absolute conductivities, and more importantly, yields relative *d-d* photoconductivity quantum efficiencies (QE) on a per-Co^{2+} basis. As shown in the supplementary information (see [53]), the data analyzed in this way are essentially independent of the specific energy at which the PC data are normalized (outside the *d-d* band), and are independent of the absolute resistivity of the film. Remarkably, the *d-d* photoconductivity QE *decreases* rapidly with increasing *x* (Fig. 4c,d). Plotting the photoconductivity QE in the $^4T_1(P)$ energy range vs *x* (Fig. 4d) shows that this trend is roughly linear in *x*. Extrapolating to zero allows estimation that the room-temperature *d-d* photoconductivity QE reaches zero when $x \approx 0.12 \pm 0.02$. This result is consistent with the absence of $^4A_2 \rightarrow {}^4T_1(P)$ *d-d* photoconductivity at $x = 0.26$ reported recently.[23] We note that some of the photoconductivity in this *d-d* energy window does not come from *d-d* excitation, however, but comes from a broad photoconductivity tail whose contribution increases as *x* increases. At $x = 0.11$, this broad tail accounts for almost all of the measured photoconductivity in this energy region (Fig. 4c). This tail is attributed to direct excitation of the $Co^{2+/3+}$ donor-type photoionization transition. The actual *d-d* contribution to photoconductivity in this *d-d* energy range is thus smaller than represented in Fig. 4d.

Phenomenologically, the product of the LHE and QE curves from Fig. 4b,d should yield the experimental *x*-dependence of the incident photon-to-current conversion efficiency of $Zn_{1-x}Co_xO$ for excitation in the *d-d* energy range (IPCE ∝ LHE*QE). This product function maximizes at $x \sim 0.06$, in good agreement with experimental IPCE trends.[10,20,21] Because of the PC normalization procedure, this trend cannot arise from overall changes in film conductivity due to scattering or phase segregation. Indeed, photoconductivity spectra of $Zn_{1-x}Co_xO$ films with similar *x* values but very different absolute resistivities yield the same relative *d-d* QE (see [53]), showing that the *d-d* photoconductivity trends identified here do not depend on absolute

resistivity. Instead, these results strongly suggest that the *x*-dependence of the *d-d* photoactivity noted empirically[10,20,21] and seen in Fig. 4c,d is an intrinsic feature of the $Zn_{1-x}Co_xO$ electronic structure.

To explore the trend seen in Fig. 4c,d in greater detail, we examined the temperature dependence of $Zn_{1-x}Co_xO$ photoconductivity as a function of *x*. Figure 5 shows photoconductivity action spectra of $Zn_{1-x}Co_xO$ films with x = 0.008, 0.04, 0.07, and 0.11, collected at various temperatures between room temperature and ~50 K. The spectra have again been normalized at 2.8 eV, compensating for changes in conductivity with temperature.

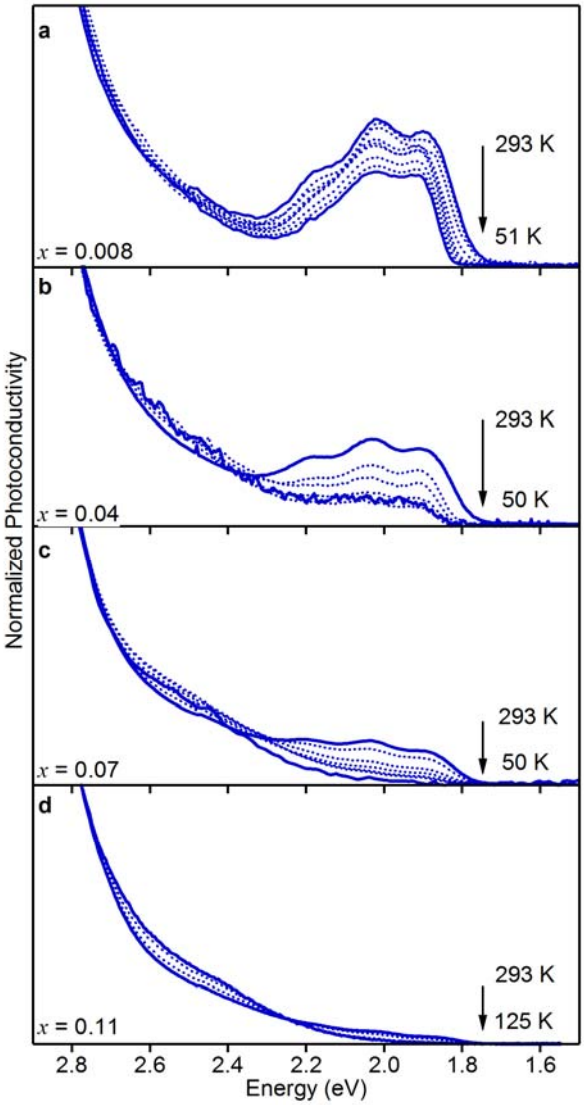

FIG. 5. Variable-temperature photoconductivity spectra of **(a)** *a*-$Zn_{0.992}Co_{0.008}O$ (measured at 293, 265, 230, 175, 154, 125, 100, 76, and 51 K), **(b)** *a*-$Zn_{0.96}Co_{0.04}O$ (measured at 293, 175, 148, 130, 100, and 48 K) **(c)** 0.07 *a*-$Zn_{0.93}Co_{0.07}O$ (measured at 293, 250, 205, 175, 125, 100, and 50 K), and **(d)** *a*-$Zn_{0.89}O_{0.11}O$ (measured at 293, 275, 250, 225, 200, 175, 150, and 125 K), all normalized at 2.8 eV.

The integrated photoconductivities in the *d-d* energy range of each spectrum in Fig. 5 are plotted vs temperature in Fig. 6. In all four films, the $^4A_2 \rightarrow {}^4T_1(P)$ photoconductivity increases as the temperature is raised, but to a different extent in each case. The x = 0.008 film's photoconductivity spectrum shows the distinctive structure of the $^4A_2 \rightarrow {}^4T_1(P)$ *d-d* band even at the lowest experimental temperature (50 K), indicating that ionization from the $^4T_1(P)$ manifold

is spontaneous ($\Delta G < 0$) at this temperature. In the other extreme, the $^4T_1(P)$ feature in the x = 0.11 film is difficult to observe at any temperature below 175 K, and is only faintly apparent even at room temperature. The observation of both spontaneous and thermally assisted ionization at x = 0.008 indicates the presence of an activation barrier (E_a) to ionization from the $^4T_1(P)$ state.[22]

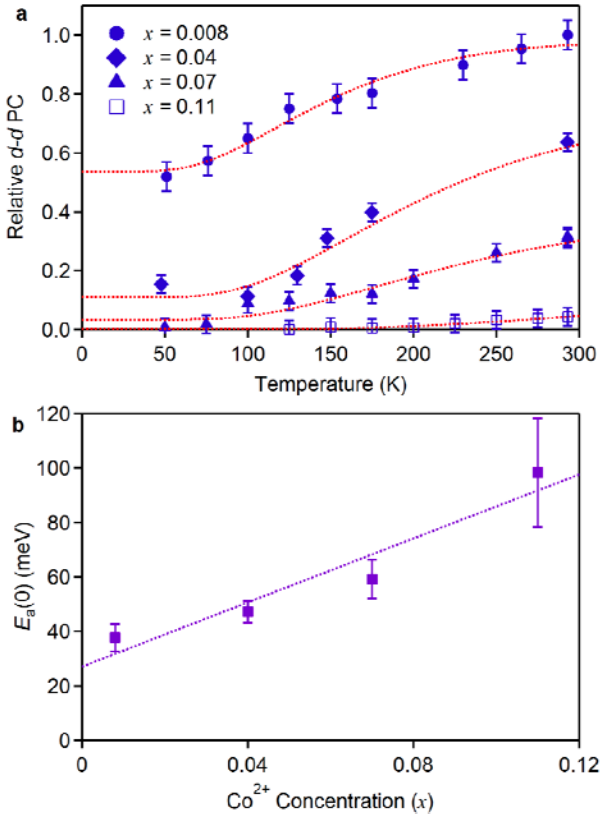

FIG. 6. (a) Temperature dependence of the integrated *d-d* photoconductivity from the spectra in Fig. 5. The dotted lines show fits of these data obtained using eqs 1 and 2, yielding activation energies for ionization from the $^4T_1(P)$ *d-d* excited state of $E_a(0)$ = 33.6 meV (x = 0.008), 46.2 meV (0.04), 51.9 meV (0.07), and 94.3 meV (0.11). **(b)** The $E_a(0)$ values determined from panel a, plotted vs x. The line shows a best linear fit to the data points, where $E_a(0, x) = (588x + 27)$ meV.

We propose that these trends in *d-d* photoconductivity ultimately derive from an x-dependence of the ZnO conduction-band-edge potential, which manifests itself as an x-dependent

energy difference between $^4T_1(P)$ and $Co^{2+/3+}$-photoionization electronic excited states. As described in Fig. 1, our experiments and previous results have demonstrated an *x*-dependence of the $Zn_{1-x}Co_xO$ energy gap ($E_g \approx (3.4 + 3.0x)$ eV),[43,46] much of which should derive from changes in the conduction band due to replacement of Zn^{2+} with Co^{2+} (see Fig. 1). This *x*-dependence impacts both the thermodynamic driving force for Co^{2+} ionization and the ionization kinetics. The data in Fig. 6a were modeled using an Arrhenius expression (eq 1) to describe the temperature-dependent transition probability for $^4T_1(P)$ ionization (*i.e.*, the transition between the Co^{2+} $^4T_1(P)$ and $Co^{2+/3+}$ ionization potential energy surfaces). To account for the temperature dependence of the conduction-band-edge potential, the temperature dependence of the activation barrier to donor-type ionization from the $^4T_1(P)$ state ($E_a(T)$) is described using the known[54-56] Varshni-like temperature dependence of the ZnO energy gap modified to reflect only the shift in the conduction band.[22] We assume that all samples are describable using the same known Varshni behavior of ZnO.

$$I(T) = I(0) + A \times \exp[-E_a(T)/kT] \quad (1)$$

$$E_a(T) = E_a(0) - 0.68 \times \left(\frac{5.5 \times 10^{-4} T^2}{440 + T} \right) \quad (2)$$

The data in Fig. 6a were fitted to eqs 1 and 2 with $E_a(0)$ and the scaling pre-factor (A) as the only adjustable parameters. $E_a(T)$ (and hence also $E_a(0)$) is defined by the curvature of the photoconductivity temperature dependence and is relatively independent of A. The fitting results are plotted in Fig. 6. From these analyses, the barrier to $^4T_1(P)$ ionization increases continuously from $E_a(0)$ = 38 ± 5 meV (x = 0.008) to 98 ± 17 meV (x = 0.11) over this series of concentrations, as plotted in Fig. 6b. The trend line fit to these activation energies is also shown in Fig. 6b and follows $E_a(0, x) = (588x + 27)$ meV.

These results provide strong evidence confirming that the unusual x-dependence of *d-d* photoconductivity in $Zn_{1-x}Co_xO$ derives from an intrinsic change in electronic structure. We propose that this change involves a shift in the conduction-band-edge potential of ZnO upon substitution of Zn^{2+} host cations by Co^{2+} impurity cations. It is well established that the energy of the first excitonic feature of ZnO increases with increasing x in $Zn_{1-x}Co_xO$, $Zn_{1-x}Mn_xO$, and $Zn_{1-x}Mg_xO$ (*e.g.*, see Fig. 1a).[43,45,57] Because cation substitution predominantly influences the conduction band (which is primarily cation 4*s* in its orbital composition), the blue shift of the exciton is largely due to a comparable shift in the conduction-band-edge potential. As a result of the rising conduction band potential, the $Co^{2+/3+}$ donor-type ionization also shifts to higher energy with increasing x. In contrast, the highly localized $^4A_2 \rightarrow {}^4T_1(P)$ *d-d* transition energy remains almost constant over this concentration range,[45] making transfer of an electron from photoexcited Co^{2+} to the conduction band less favorable at higher x.

From these observations, a phenomenological ionization coordinate diagram is proposed (Fig. 7) whose key features are the relative energies of the $^4T_1(P)$ and $Co^{2+/3+}$ ionization states (ΔE_0) and the energy barrier (E_a) between them, both of which depend on x. At $x = 0.008$, the $^4T_1(P)$ manifold resides above the $Co^{2+/3+}$ ionization threshold at 50 K (small x in Fig. 7), meaning donor-type ionization is spontaneous from this excited state. Thermal energy assists this ionization, but is not required, *i.e.*, it improves the ionization *kinetics*. By $x \sim 0.11$, spontaneous ionization is no longer observed at 50 K, and the $Co^{2+/3+}$ ionization threshold appears to have shifted above the $^4T_1(P)$ manifold at low temperatures (large x in Fig. 7). A small amount of photoconductivity is recovered at room temperature for this concentration. The balance between the x-dependent electronic structure and the x-dependent light harvesting efficiency leads to a maximum in the experimental *d-d* photoresponse of $Zn_{1-x}Co_xO$ at $x \approx 0.06$. This observation

suggests that bandgap engineering to lower the ZnO conduction-band-edge potential, for example by Cd^{2+} alloying, should shift the maximum photoresponse to greater x and substantially improve the visible-light photosensitivity of this material.

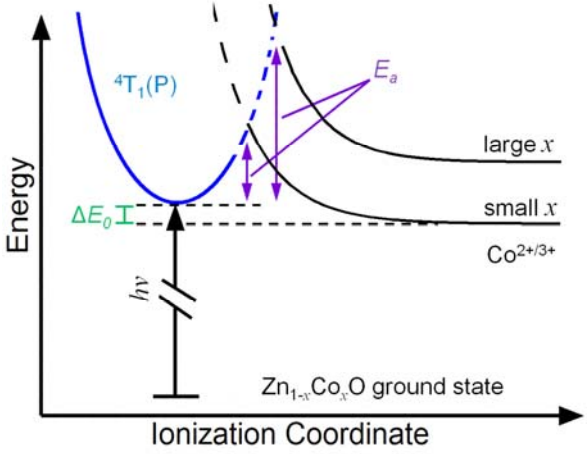

FIG. 7. Schematic depiction of the electronic coupling between the $^4T_1(P)$ and $Co^{2+/3+}$ photoionization potential energy surfaces. Both direct and thermally assisted photoconductivity is observed following $^4T_1(P)$ excitation. Thermally assisted photoconductivity is diminished at high x, where the conduction-band edge has moved higher in energy, and at low temperatures.

Summary

The $^4A_2 \rightarrow {}^4T_1(P)$ *d-d* photoconductivity of $Zn_{1-x}Co_xO$ shows a strong dependence on x, maximizing at $x \sim 0.06$ despite much greater solid solubilities of Co^{2+} in this lattice and continued increases in *d-d* absorbance with increasing x. Variable-temperature photoconductivity measurements performed on high-quality epitaxial films of $Zn_{1-x}Co_xO$ as a function of x provide a microscopic explanation of this concentration dependence. The data show that increasing x increases the energy of the conduction-band edge, which raises the $Co^{2+/3+}$ ionization energy relative to the $^4T_1(P)$ state. At $x = 0.008$, ionization from the $^4T_1(P)$ state proceeds at all temperatures, but increasing to $x = 0.11$ eliminates *d-d* photocurrent at low temperatures and makes it very ineffective at room temperature. At all Co^{2+} concentrations between $x = 0.008$ and

$x = 0.11$, $Zn_{1-x}Co_xO$ shows thermally assisted ionization following $^4T_1(P)$ excitation, but this also becomes much less effective with increasing x.

In a broader context, the findings here for $Zn_{1-x}Co_xO$ improve our understanding of the rich electronic structures that can arise from the introduction of transition-metal impurity ions into wide-gap semiconductors in general, and provide a foundation for studying the contributions of mid-gap dopant-centered electronic excited states to the electronic structures and physical properties of related doped semiconductors. The fact that the strong *d-d* absorption of $Zn_{1-x}Co_xO$ can generate visible-light photoactivity via sensitization of a nearby photoionization state implies similar interpretations for other reported cases of mid-gap *d-d* photoactivity in doped oxides.[3,6,10] The question arises whether inter-dopant sensitized ionization can be achieved in co-doped oxides, which could provide a mechanism for separating light absorption from charge separation to improve overall photoactivity. Finally, the present results highlight the need for accurate experimental and theoretical assessment of the energies and intensities of mid-gap dopant-centered photoionization transitions, and the responses of such transitions to such basic parameters as temperature and alloy composition. Among the rich electronic transitions displayed by doped semiconductors, photoionization transitions have the greatest impact on photochemistry, photoelectrochemistry, photoconductivity, and even magnetism, yet remain the least thoroughly explored.

Acknowledgments

This work was supported by the US National Science Foundation (CHE 0628252-CRC). A portion of the research was performed using EMSL, a national scientific user facility sponsored by the Department of Energy's Office of Biological and Environmental Research located at

PNNL. Work at EMSL was supported by the U.S. Department of Energy, Office of Science, Office of Basic Energy Sciences, Division of Materials Science and Engineering Physics.

References

[1] W. Y. Choi, A. Termin, and M. R. Hoffmann, J. Phys. Chem. **98**, 13669 (1994).
[2] N. Serpone, D. Lawless, J. Disdier, and J.-M. Herrmann, Langmuir **10**, 643 (1994).
[3] Z. Zou, J. Ye, K. Sayama, and H. Arakawa, Nature **414**, 625 (2001).
[4] S. Klosek and D. Raftery, J. Phys. Chem. B **105**, 2815 (2001).
[5] C. Lettmann, H. Hinrichs, and W. F. Maier, Angew. Chem. Int. Ed. **40**, 3160 (2001).
[6] H. Kato and A. Kudo, J. Phys. Chem. B **106**, 5029 (2002).
[7] G. R. Torres, T. Lindgren, J. Lu, C. G. Granqvist, and S. E. Lindquist, J. Phys. Chem. B **108**, 5995 (2004).
[8] R. Konta, T. Ishii, H. Kato, and A. Kudo, J. Phys. Chem. B **108**, 8992 (2004).
[9] R. Nakamura, T. Tanaka, and Y. Nakato, J. Phys. Chem. B **108**, 10617 (2004).
[10] T. F. Jaramillo, S.-H. Baeck, A. Kleiman-Shwarsctein, K.-S. Choi, G. D. Stucky, and E. W. McFarland, J. Comb. Chem. **7**, 264 (2005).
[11] W. K. Liu, G. M. Salley, and D. R. Gamelin, J. Phys. Chem. B **109**, 14486 (2005).
[12] Q. Xiao, J. Zhang, C. Xiao, and X. K. Tan, Mater. Sci. Eng. B-Solid State Mater. Adv. Technol. **142**, 121 (2007).
[13] W. Zhu, X. Qiu, V. Iancu, X.-Q. Chen, H. Pan, W. Wang, N. M. Dimitrijevic, T. Rajh, H. M. Meyer, M. P. Paranthaman, G. M. Stocks, H. H. Weitering, B. Gu, G. Eres, and Z. Zhang, Phys. Rev. Lett. **103**, 226401 (2009).
[14] Y. Gai, J. Li, S.-S. Li, J.-B. Xia, and S.-H. Wei, Phys. Rev. Lett. **102**, 036402 (2009).
[15] Y. Kanai, J. Phys. Soc. Jpn. **24**, 956 (1968).
[16] M. Jakani, G. Campet, J. Claverie, D. Fichou, J. Pouliquen, and J. Kossanyi, J. Sol. State Chem. **56**, 269 (1985).
[17] D. Fichou, J. Pouliquen, J. Kossanyi, M. Jakani, G. Campet, and J. Claverie, J. Electroanal. Chem. **188**, 167 (1985).
[18] K. Kobayashi, T. Maeda, S. Matsushima, and G. Okada, J. Mater. Sci. **27**, 5953 (1992).
[19] K. Kobayashi, T. Maeda, S. Matsushima, and G. Okada, Jpn. J. Appl. Phys. **31**, L1079 (1992).
[20] L. Bahadur and T. N. Rao, Sol. Energy Mat. Sol. Cells **27**, 347 (1992).
[21] T. Hirano and H. Kozuka, J. Mater. Sci. **38**, 4203 (2003).
[22] C. A. Johnson, T. C. Kaspar, S. A. Chambers, G. M. Salley, and D. R. Gamelin, Phys. Rev. B **81**, 125206 (2010).
[23] S. G. Gilliland, J. A. Sans, J. F. Sánchez-Royo, G. Almonacid, and A. Segura, Appl. Phys. Lett. **96**, 241902 (2010).
[24] N. V. Joshi, *Photoconductivity: Art, Science, and Technology* (Marcel Dekker, New York, 1990).
[25] R. H. Bube, *Photoconductivity of Solids* (Wiley, New York, 1960).
[26] C. J. Ballhausen, *Introduction to Ligand Field Theory* (McGraw-Hill Book Company, Inc., New York, 1962).
[27] A. Zunger, in *Solid State Physics* (Academic Press, 1986), Vol. 39, p. 275.
[28] H.-J. Schulz and M. Thiede, Phys. Rev. B **35**, 18 (1987).
[29] D. A. Schwartz and D. R. Gamelin, Adv. Mater. **16**, 2115 (2004).
[30] K. R. Kittilstved, W. K. Liu, and D. R. Gamelin, Nature Materials **5**, 291 (2006).

[31] C. D. Pemmaraju, R. Hanafin, T. Archer, H. B. Braun, and S. Sanvito, Phys. Rev. B **78**, 054428 (2008).
[32] A. Walsh, J. L. F. Da Silva, and S.-H. Wei, Phys. Rev. Lett. **100**, 256401 (2008).
[33] H. Raebiger, S. Lany, and A. Zunger, Phys. Rev. B **79**, 165202 (2009).
[34] H. Morkoç and Ü. Özgür, *Zinc Oxide: Fundamentals, Materials and Device Technologies* (Wiley-VCH, Weinheim, 2009).
[35] T. C. Kaspar, T. Droubay, Y. Li, S. M. Heald, P. Nachimuthu, C. M. Wang, V. Shutthanandan, C. A. Johnson, D. R. Gamelin, and S. A. Chambers, New J. Phys. **10**, 055010 (2008).
[36] T. C. Droubay, D. J. Keavney, T. C. Kaspar, S. M. Heald, C. M. Wang, C. A. Johnson, K. M. Whitaker, D. R. Gamelin, and S. A. Chambers, Phys. Rev. B **79**, 155203 (2009).
[37] A. Ney, K. Ollefs, S. Ye, T. Kammermeier, V. Ney, T. C. Kaspar, S. A. Chambers, F. Wilhelm, and A. Rogalev, Phys. Rev. Lett. **100**, 157201 (2008).
[38] A. Ney, M. Opel, T. C. Kaspar, V. Ney, S. Ye, K. Ollefs, T. Kammermeier, S. Bauer, K. W. Nielsen, S. T. B. Goennenwein, M. H. Engelhard, S. Zhou, K. Potzger, J. Simon, W. Mader, S. M. Heald, J. C. Cezar, F. Wilhelm, A. Rogalev, R. Gross, and S. A. Chambers, New J. Phys. **12**, 013020 (2010).
[39] F. R. S. Clark and D. J. Moffatt, Appl. Spectrosc. **32**, 547 (1978).
[40] D. A. Schwartz, N. S. Norberg, Q. P. Nguyen, J. M. Parker, and D. R. Gamelin, J. Am. Chem. Soc. **125**, 13205 (2003).
[41] H. A. Weakliem, J. Chem. Phys. **36**, 2117 (1962).
[42] P. Koidl, Phys. Rev. B **15**, 2493 (1977).
[43] M. Ivill, S. J. Pearton, S. Rawal, L. Leu, P. Sadik, R. Das, A. F. Hebard, M. Chisholm, J. D. Budai, and D. P. Norton, New J. Phys. **10**, 065002 (2008).
[44] Z. Xiao, H. Matsui, N. Hasuike, H. Harima, and H. Tabata, J. Appl. Phys. **103**, 043504 (2008).
[45] M. A. White, S. T. Ochsenbein, and D. R. Gamelin, Chem. Mater. **20**, 7107 (2008).
[46] Z. Y. Xiao, H. Matsui, N. Hasuike, H. Harima, and H. Tabata, J. Appl. Phys. **103**, 043504 (2008).
[47] W. Pacuski, D. Ferrand, J. Cibert, C. Deparis, J. A. Gaj, P. Kossacki, and C. Morhain, Phys. Rev. B **73**, 035214 (2006).
[48] Y. Z. Peng, T. Liew, W. D. Song, C. W. An, K. L. Teo, and T. C. Chong, J. Supercond., 97 (2005).
[49] K. J. Kim and Y. R. Park, Appl. Phys. Lett **81**, 1420 (2002).
[50] M. Bouloudenine, N. Viart, S. Colis, J. Kortus, and A. Dinia, Appl. Phys. Lett **87**, 052501 (2005).
[51] S. V. Bhat and F. L. Deepak, Solid State Comm. **135**, 345 (2005).
[52] X. Q. Qiu, L. O. Li, and G. S. Li, Appl. Phys. Lett **88**, 114103 (2006).
[53] See EPAPS Document No. [number will be inserted by publisher] for additional data and characterization figures. For more information on EPAPS, see http://www.aip.org/pubservs/epaps.html.
[54] O. Madelung, *Semiconductors: Data Handbook* (Springer, Berlin, 2004).
[55] B. K. Meyer, H. Alves, D. M. Hofmann, W. Kriegseis, D. Forster, F. Bertram, J. Christen, A. Hoffmann, M. Straßburg, M. Dworzak, U. Haboeck, and A. V. Rodina, Phys. Stat. Sol. (b) **241**, 231 (2004).
[56] C. J. Youn, T. S. Jeong, M. S. Han, and J. H. Kim, J. Cryst. Growth **261**, 526 (2004).

[57] T. H. Kim, J. J. Park, S. H. Nam, H. S. Park, N. R. Cheong, J. K. Song, and S. M. Park, Appl. Surf. Sci. **255**, 5264 (2009).